Supporting Information

Regulating solvation structure and absorption behavior on zinc anode by polar organic molecules to achieve durable dendrite-free zinc metal anodes for aqueous zinc-ion batteries

Xiaoqin Zhang[1], Haoran Lang[1], Chao Li[2], Min Li[1], Bin Xie[1], Ji Chen[1], Yuxiang Chen[1], Yu Huo[1], Lin Li[2], Qiaoji Zheng[1 *], Xin Tan[2 *], Heng Zhang[3 *], Dunmin Lin[1 *]

[1]College of Chemistry and Materials Science, Sichuan Normal University, Chengdu 610066, China

[2]Institute for Carbon Neutralization Technology，College of Chemistry and Materials Engineering, Wenzhou University, Wenzhou, Zhejiang 325035, China

[3]School of Materials Science and Engineering, Suzhou University of Science and Technology, Suzhou 215009, China

[*]Corresponding authors: joyce@sicnu.edu.cn (Qiaoji Zheng); xintan@wzu.edu.cn (Xin Tan); zhangheng@usts.edu.cn (Heng Zhang); ddmd222@sicnu.edu.cn (Dunmin Lin); Fax: +86 28 84760802 Tel: +86 2884760802

Experimental

1. Preparation of electrolytes

Zinc sulfate ($ZnSO_4 \cdot 7H_2O$, Cologne, 99%) was dissolved in deionized water (DI water) to obtain a 2 M $ZnSO_4$ baseline electrolyte. Cyclen ($C_8H_{20}N_4$, Macklin, 98%) with different concentrations (5 g/L, 10 g/L, 15 g/L) was added to 2 M $ZnSO_4$ electrolyte to obtain Cy-containing electrolytes. The optimal concentration of Cy was 10 g/L.

2. Preparation of electrodes

The purchased Zn foil (thickness: 20 μm, 100 μm, 99.99%) was polished to remove the oxidation layer, and then cut into discs (φ = 10 mm) to be used as Zn electrodes.

VO_2 nanosheets were prepared by a hydrothermal method. 2 mmol of ammonium metavanadate was dissolved in 15 mL of DI water under magnetic stirring, and then 3 mmol of oxalic acid solution was added and stirred for 30 min. The obtained mixture was transferred to a 100 mL autoclave lined with PTFE and kept at 180 °C for 24 h. Subsequently, the synthesized powders were washed several times with ethanol and DI water and dried in a vacuum oven for one day to obtain VO_2 powders. The positive electrode was prepared by mixing VO_2 powders, acetylene black and polyvinylidene fluoride (PVDF) in a mass ratio of 7:2:1 with 1-Methyl-2-pyrrolidinone (NMP, Macklin,99%) as solvent, and then the slurry was casted on a titanium foil. After drying in vacuum at 70 °C overnight, the electrode with VO_2 was obtained. (Cathode loading: 1 mg/cm^2)

3. Materials characterizations and electrochemical properties

The X-ray diffraction analysis (XRD) of samples was characterized by the XRD equipment (Smart Lab, Riga ku, Japan) with a Cu-Kα (λ = 1.540598 Å, Smart Lab) source (scan rate of 2 min^{-1}) and 2θ ranging from 10° to 80°. The morphology of the samples was studied by field emission scanning electron microscopy (SEM, FEI, Sirion 200). The elemental analysis of the samples was carried out using field emission scanning electron microscopy (SEM, FEI-Quanta 250, USA) with energy dispersive x-ray (EDX) elemental mapping.

All tested CR2032-type coin cells were assembled in air environment, and the amount of electrolyte used in the coin cells was 200 μL. The VO_2//Zn full cell was assembled with the Zn foil (thickness: 100 μm) as the anode and VO_2 as the cathode. The CV was tested in the electrolytic cell with Ti plate as the working electrode, Pt plate as the reverse electrode and Ag/AgCl as the reference electrode. With Zn plate as the working electrode, Pt plate as the reverse electrode and Ag/AgCl as the reference electrode, the LSV and Tafel diagrams were measured in the electrolytic cell. The CA is obtained by Amperometric i-t Curve testing with Zn plate as the working electrode, Pt plate as the reverse electrode, and Zn plate as the reference electrode at a voltage of −150 mV. The electrochemical impedance spectroscopy (EIS) of the cells were conducted on the frequency range of 100 kHz to 1 Hz. The above tests were performed on an electrochemical workstation (CHI760E, CHI660E, Shanghai, China). With zinc plate as anode, 20 μm copper foil as cathode and glass fiber as diaphragm, a zinc-copper

half battery was assembled and CE test was carried out on the Land CT5001A battery test device.

A self-made optical Zn||Zn battery was designed for in-situ observation of zinc deposition in different electrolytes. The transparent Zn||Zn cell consists of a zinc plate and a glass dish. The zinc plate is fixed to the glass at the bottom of the glass dish, and then the electrolyte is added to the glass dish, so that the solution is immersed in the zinc plate. The transparent Zn||Zn cell was tested for Zn stripping/plating using a cell tester (LAND, China) at a current density of 20 mA cm^{-2}, in which a video camera (NSZ-808) was used to observe and record the growth of Zn dendrites.

4. MD Simulations

Molecular dynamics (MD) simulations were run using LAMMPS[1, 2]. The initial configuration of the system was established using PACKMOL[3]and Moltemplate (http://www.moltemplate.org/). A periodic box of dimensions 30×30×30$Å^3$ was used for the system. For the 2 M $ZnSO_4$-Cyclen, a blank group has 40 $ZnSO_4$ molcules, and 1200 H_2O molecules. In the experimental group, based on the former, an additional 20 Cyclen molecules were added. The force field parameters for the solvent were derived from the GAFF2 force field of ACPYPE[4]while the force field for the salt was sourced from (https://doi.org/10.1063/1.5121392). The TIP3P model was utilized for the water force field. An 12Å LJ cut-off and a particle-particle-particle-mesh (PPPM) solver for long-range Coulombic interactions were also employed in our simulations. First，all the systems were first submitted to energy minimization by using the conjugate

gradient(CG)method. Then, they were heated from 10 to 298 K in 1ns, followed by 2000ps equilibration under isothermal-isobaric ensemble (NPT). Then the NVT runs were 40ns long at 298K. The visualization of the electrolyte structure was achieved through VMD[5].

5. Density functional theory (DFT) calculation for solvated structure of the hydrated Zn^{2+}.

DFT calculations were conducted in Gaussian09 program. Electrostatic potential (ESP) was obtained from the Multiwfn3.8[6, 7]and VMD1.9.3[5]software packages， and the electrostatic potential involved in the analyses was evaluated by Multiwfn based on the highly effective algorithm proposed in Ref[7]. The geometries of Cyclen, SO_4^{2-}, and H_2O were optimized under the framework of DFT with B3LYP-D3(BJ)/def2-TZVP[8, 9] and the universal solvation model SMD[10] was used to simulate the aqueous environment. Then use the same functional and basis set to calculate the single point energy and binding energy of the optimized structure. The binding energy of the complex was calculated from the formula: “E(Binding Energy)=E(AB)-E(A)-E(B)”,where E(AB), E(A), and E(B) denote the total energies of the AB complexes, bare A, and bare B, respectively.

6. DFT calculation for H_2O/Cy on the Zn(002).

All of the spin-polarized DFT calculations were performed using the VASP program[11-13], which uses a plane-wave basis set and a projector augmented wave method (PAW) for the treatment of core electrons[12]. The Perdew, Burke, and

Ernzerhof exchange-correlation functional within a generalized gradient approximation (GGA-PBE)[14] was used in our calculations, and the van der Waals (vdW) correction proposed by Grimme (DFT-D3)[15] was employed due to its good description of long-range vdW interactions. For the expansion of wavefunctions over the plane-wave basis set, a converged cutoff was set to 450 eV. In geometry optimizations, all the structures were relaxed up to the residual atomic forces smaller than 0.02 eV/Å, and the total energy was converged to 10^{-5} eV. The Brillouin zone integration was performed on the (4×4×1) Monkhorst–Pack k-point mesh[16].

6.Calculation of the cumulative plating capacity

Cumulative plating capacity = current density × total Zn plating time

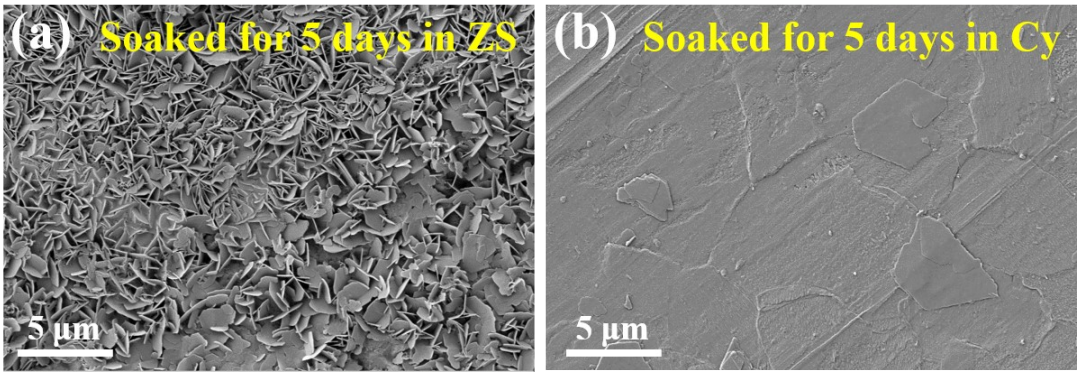

Fig. S1 SEM images of Zn soaked in (a) ZS electrolyte and (b) 10 g/L Cy-added electrolyte for 5 days.

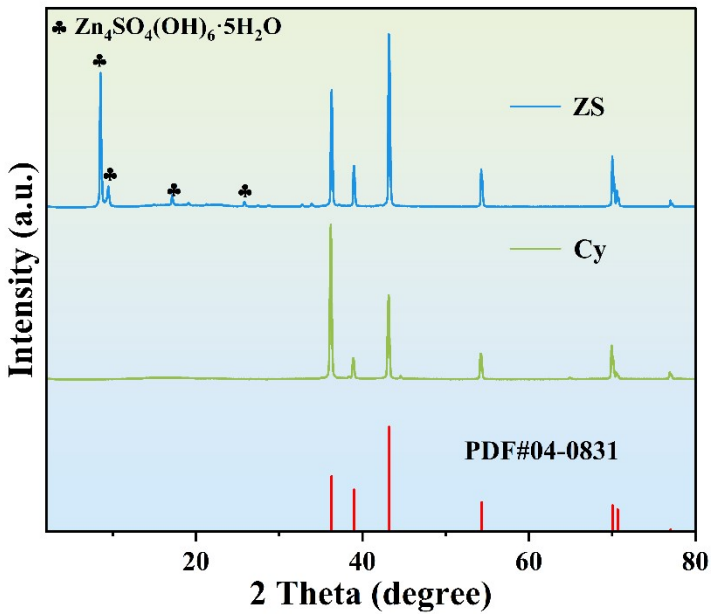

Fig. S2 XRD patterns of Zn anodes soaked for 5 days in ZS electrolytes without or with 10 g/L Cy.

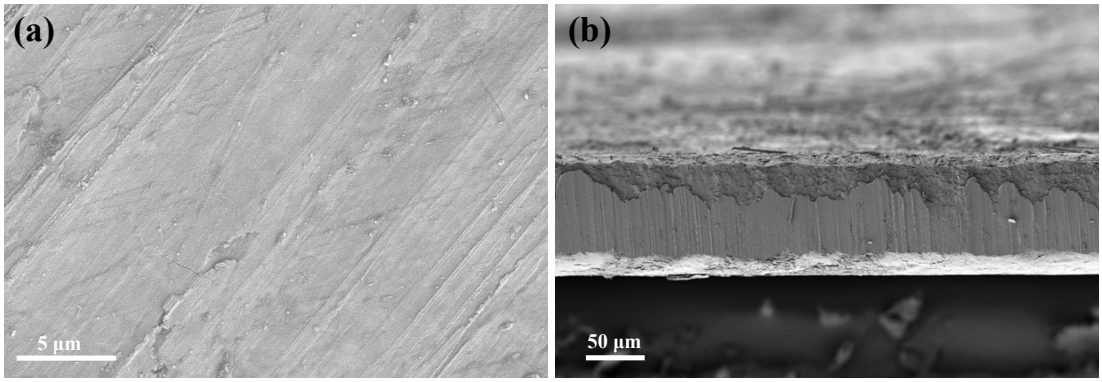

Fig. S3 SEM images of bare zinc foil: (a) surfaces and (b) cross sections.

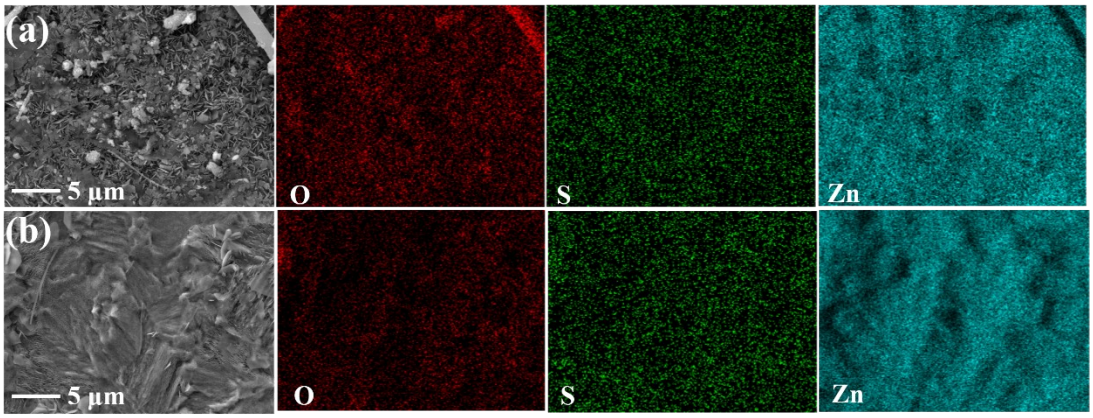

Fig. S4 SEM images and EDS mappings of surface of bare zinc foils cycled for 50 h: (a) in ZS electrolyte; (b) in 10 g/L Cy -added ZS electrolyte.

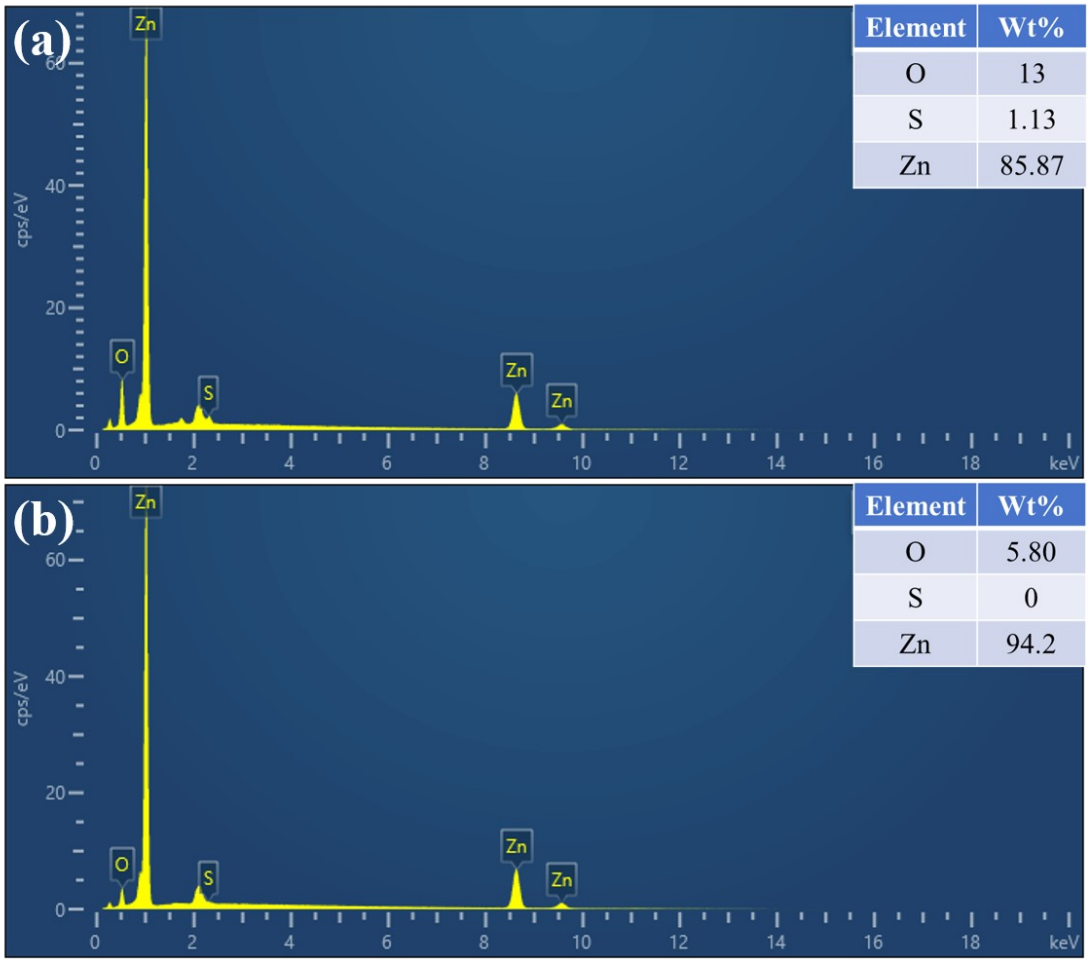

Fig. S5 EDX spectra of zinc foils cycled for 50h: (a) in ZS electrolyte; (b) in 10 g/L Cy -added ZS electrolyte.

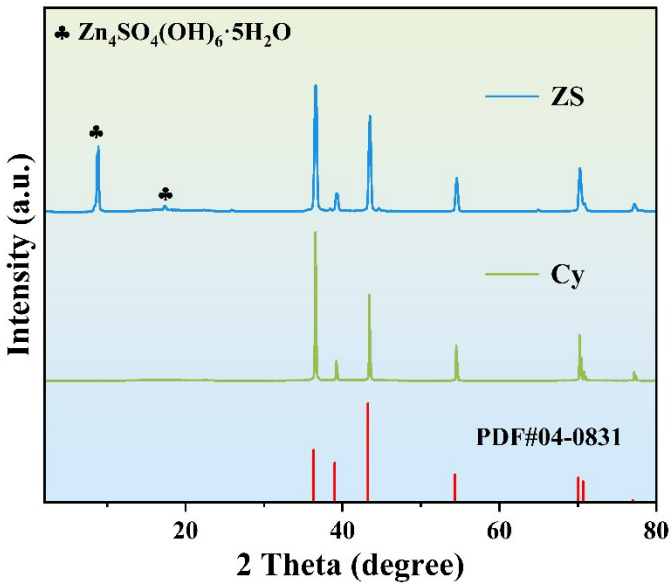

Fig. S6 XRD patterns of Zn anodes cycled for 50 h in ZS electrolytes without or with 10 g/L Cy.

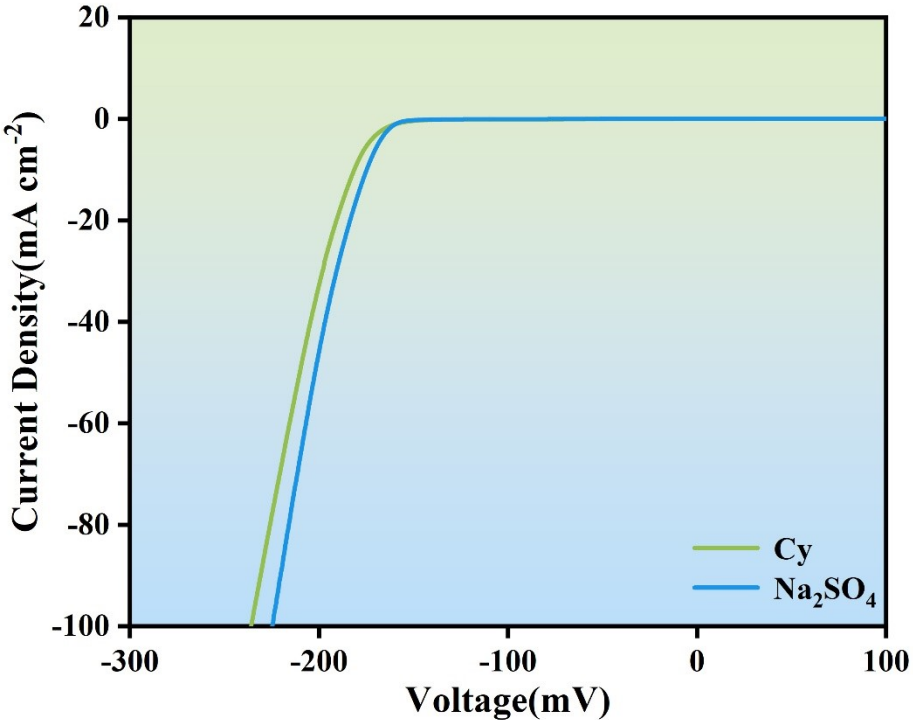

Fig. S7. Electrochemical stability windows of different electrolytes.

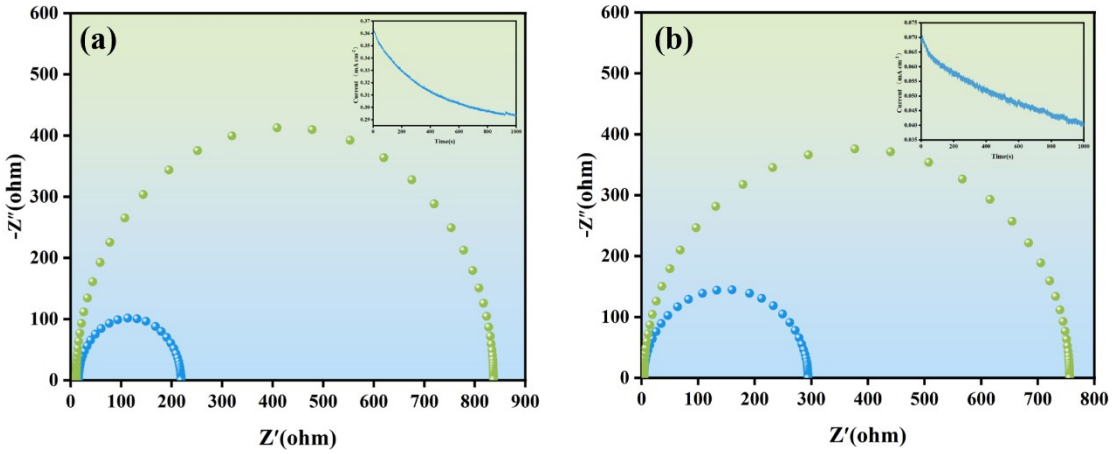

Fig. S8 Measurements of Zn^{2+} transference number. Current-time plots of Zn symmetric cells in (a) ZS and (b) 10g Cy electrolytes after polarization at a constant potential (25 mV) for 1000 s.

The transference number of Zn^{2+} (t) can be evaluated by the following equation:

$$t_{Zn^{2+}} = \frac{I_S(\Delta V - I_0 R_0)}{I_0(\Delta V - I_S R_S)}$$

where ΔV is the constant polarization voltage applied (25 mV here), I_0 and R_0 are the initial current and resistance, I_S and R_S represent the steady-state current and resistance, respectively.

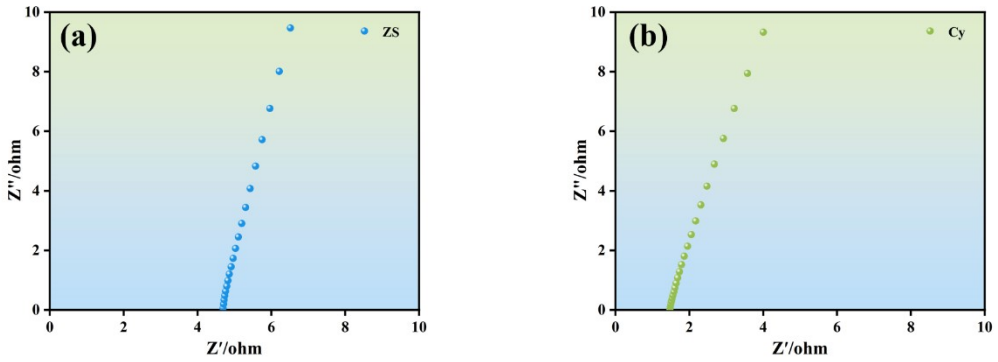

Fig. S9 EIS spectra in (a) ZS and (b) 10g Cy electrolytes.

Galvanostatic tests were performed on assembled cells using a Land CHI760E battery test system. Ionic conductivity was measured by AC impedance spectroscopy in the frequency range of 1 Hz to 100 kHz. The electrochemical cell configuration consisted of the two electrolytes to form a structure of "Ti | electrolyte | Ti." Ionic conductivity σ was calculated according to the following equation:

$$\sigma = \frac{L}{AR_b}$$

where L is the thickness of the glass microfiber filters membrane, defining the distance between the two Ti electrodes as 0.042 cm, and A is the area of the electrode as 2.011 cm^2. Resistance (R_b) was taken at the intercept of the Nyquist plot with the real axis of the impedance spectra.

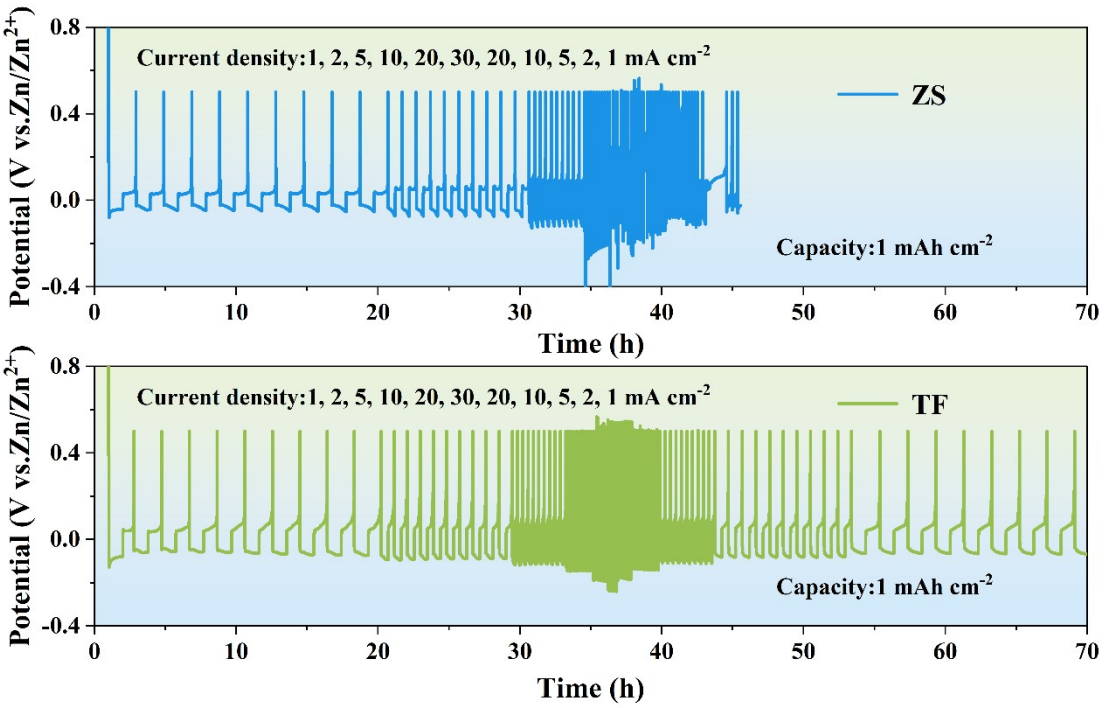

Fig. S10 Rate performance of Zn//Cu cells using (a)ZS electrolyte and (b)10 g/L Cy-added ZS electrolyte at different current densities from 1 to 30 mA cm^{-2}.

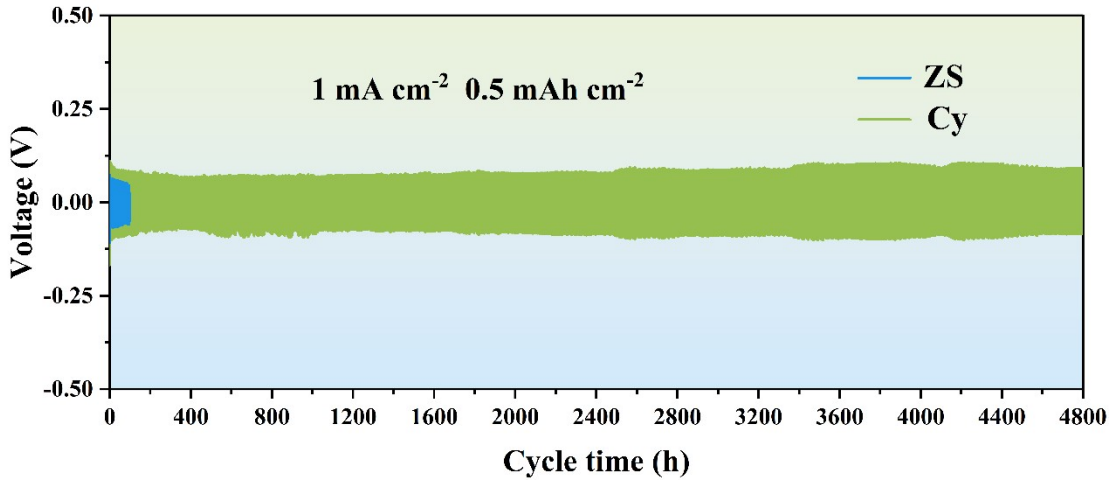

Fig. S11 Long-term cycle test of Zn||Zn symmetric batteries in different electrolytes at 1 mA cm^{-2}/0.5 mAh cm^{-2}.

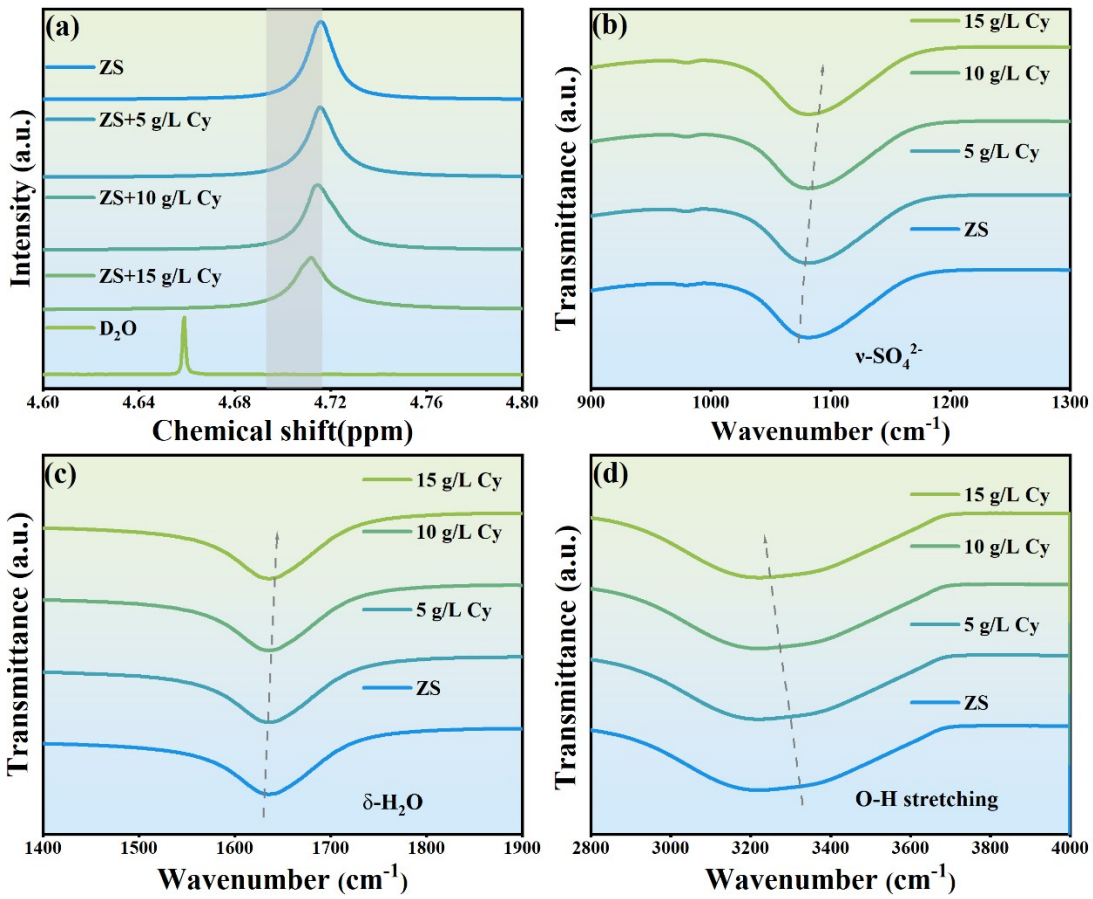

Fig. S12 (a) NMR of 1H of electrolytes with different Cy concentrations; (b-d) FT-IR spectra of ZS electrolytes with different Cy contents.

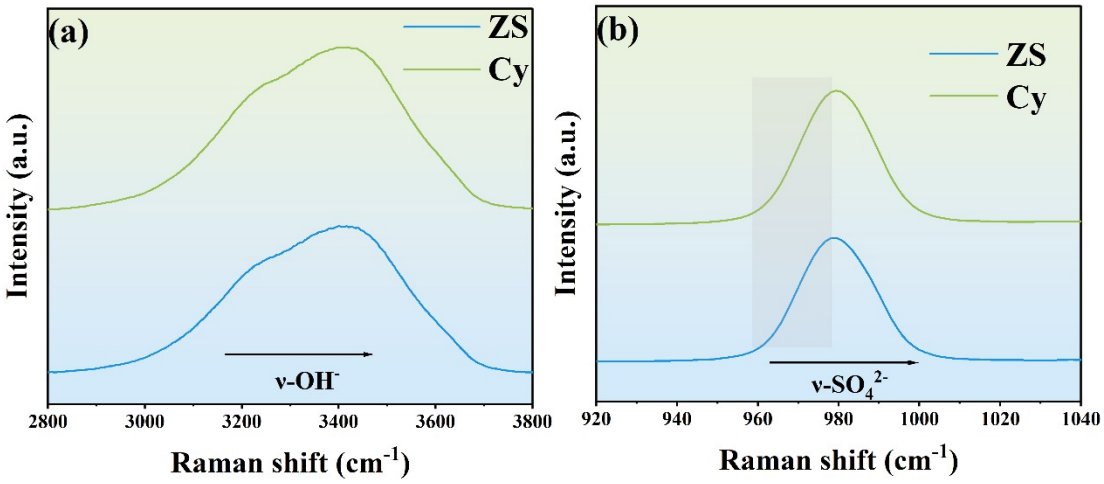

Fig. S13 (a-b) Raman spectra of ZS solution without/with 10g/L Cy.

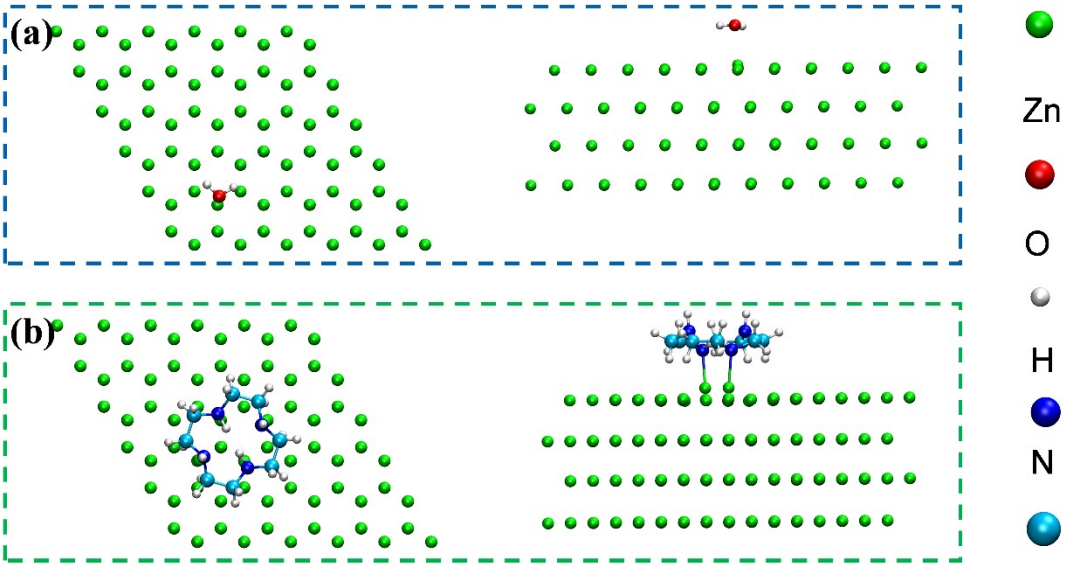

Fig. S14 Adsorption energies of H_2O and Cy molecules on the Zn(002) crystal plane of Zn metal.

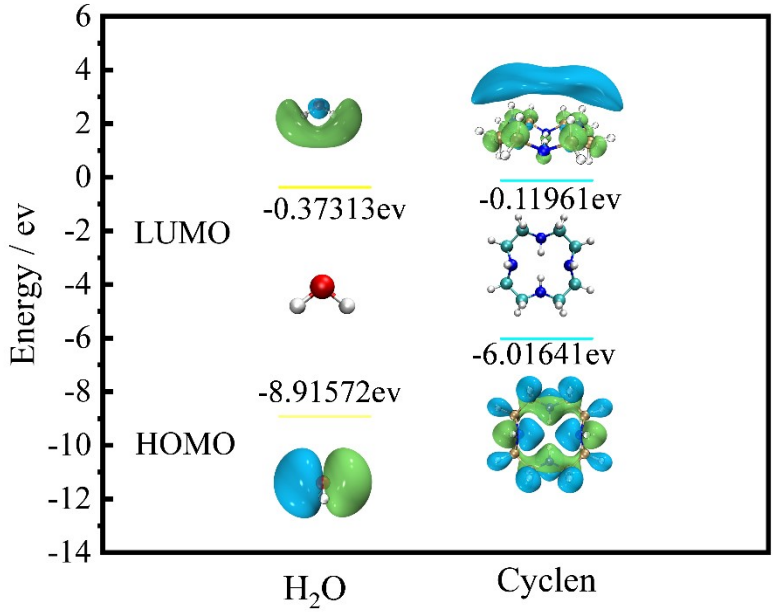

Fig. S15 LUMO, HOMO is surfaces of H_2O (left) and Cy (right) molecules.

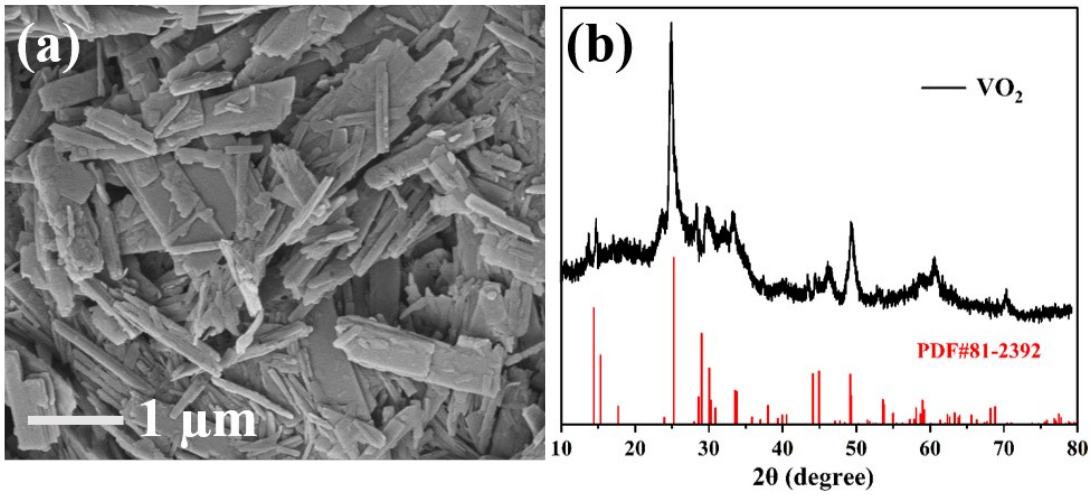

Fig. S16 (a) XRD pattern of VO_2; (b) SEM image of VO_2.

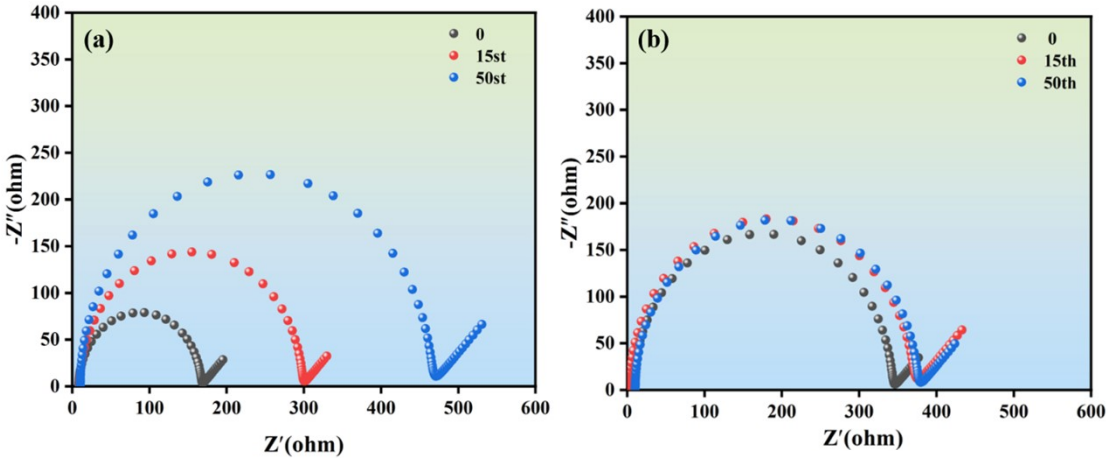

Fig. S17 (a) EIS of different cycles without Cy additive (b) EIS of different cycles with Cy additive

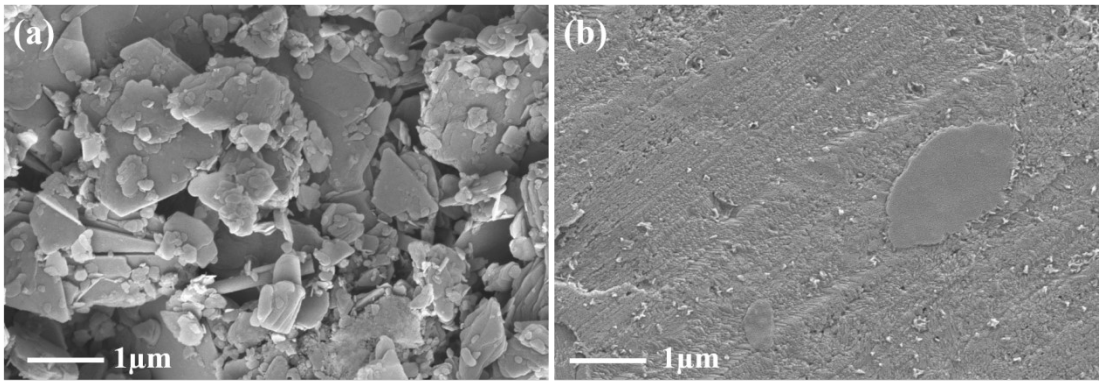

Fig S18 SEM images of Zn electrodes for Zn//VO_2 full cells cycled for 100 cycles in (a) ZS electrolytes and (b) 10 g/L Cy-added ZS electrolytes.

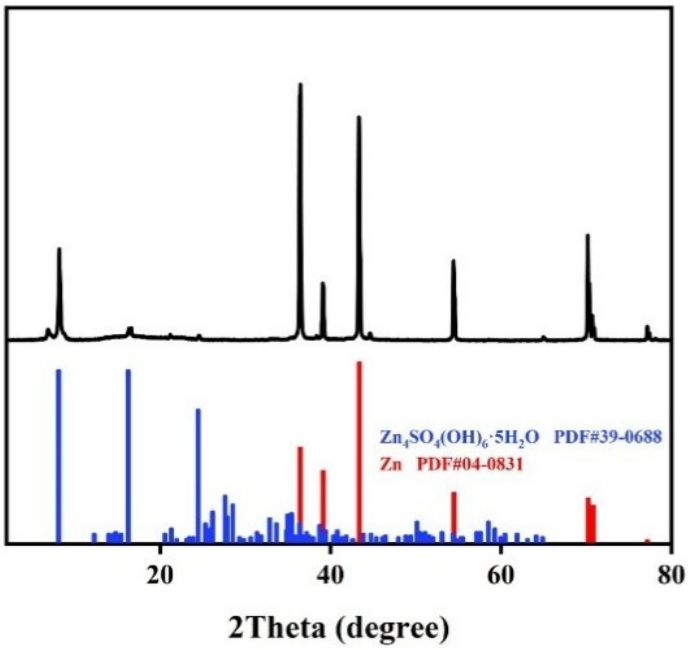

Fig. S19 XRD of Zn after 100 cycles

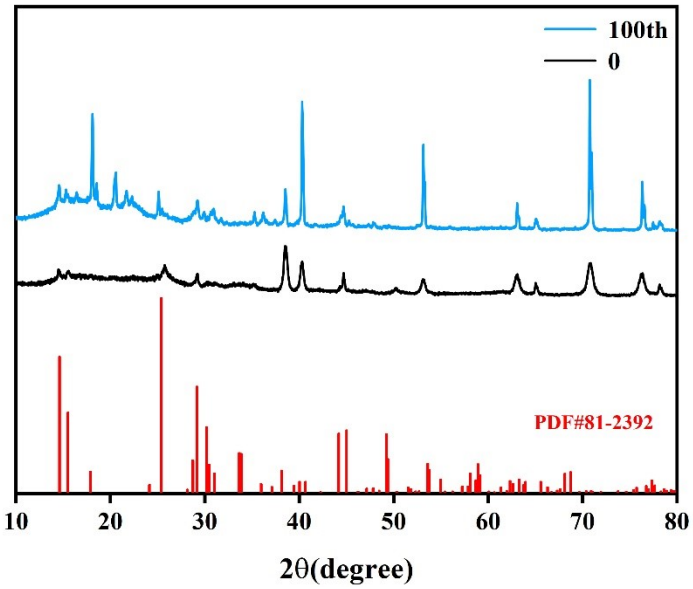

Fig. 20 XRD of VO_2 after uncyclic and circulating 100 cycles

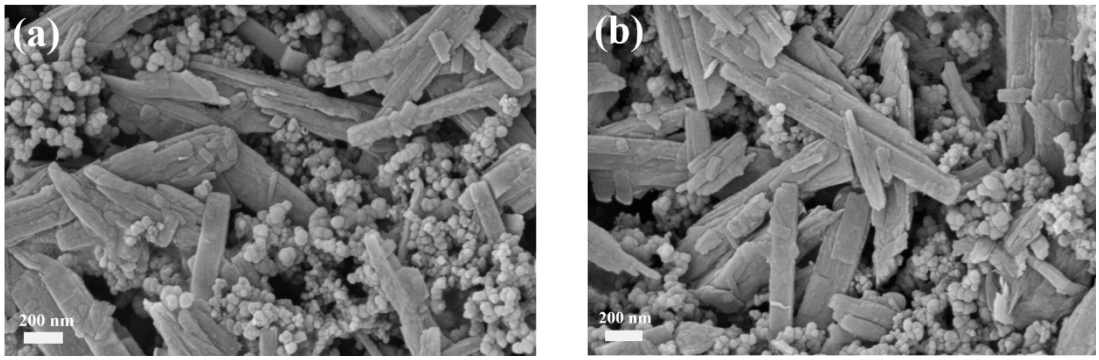

Fig. 21 (a) SEM of original VO_2 (b) SEM of VO_2 after 100 cycles

Table S1. Comparison of the electrochemical properties of recently reported Zn||Zn symmetric cells in Zn-ion batteries with the present work.

Modified materials	Current density with capacity	Cycle life	Ref.
Cy	2mA cm^{-2} with 1mAh cm^{-2}	4000h	**This work**
DG	1mA cm^{-2} with 0.5mAh cm^{-2}	3500h	[17]
DMSO	0.5mA cm^{-2} with 0.5mAh cm^{-2}	1000h	[18]
PG	0.5mA cm^{-2} with 0.5mAh cm^{-2}	3500h	[19]
Azi	1mA cm^{-2} with 1mAh cm^{-2}	4000h	[20]
Coumarin	5mA cm^{-2} with 5mAh cm^{-2}	400h	[21]
ggg	2mA cm^{-2} with 2mAh cm^{-2}	1400h	[22]
Ace	1mA cm^{-2} with 1mAh cm^{-2}	3000h	[23]
TBP	2mA cm^{-2} with 1mAh cm^{-2}	2100h	[24]
DTPA-Na	2mA cm^{-2} with 1mAh cm^{-2}	800h	[25]
CTAB	2mA cm^{-2} with 1mAh cm^{-2}	2000h	[26]
TPPS	1mA cm^{-2} with 1mAh cm^{-2}	2300h	[27]
ZnBF-VC	0.5mA cm^{-2} with 0.25mAh cm^{-2}	2200h	[28]
Me56	5mA cm^{-2} with 5mAh cm^{-2}	1000h	[29]
ZS/C_3N^+–COO^-	1mA cm^{-2} with 1mAh cm^{-2}	3500h	[30]
DDM	0.5mA cm^{-2} with 0.5mAh cm^{-2}	1400h	[31]

References

[1] S. Plimpton, Fast Parallel Algorithms for Short-Range Molecular Dynamics, J. Comput. Phys 117 (1995) 1-19.

[2] A.P. Thompson, H.M. Aktulga, R. Berger, D.S. Bolintineanu, W.M. Brown, P.S. Crozier, P.J. in 't Veld, A. Kohlmeyer, S.G. Moore, T.D. Nguyen, R. Shan, M.J. Stevens, J. Tranchida, C. Trott, S.J. Plimpton, LAMMPS - a flexible simulation tool for particle-based materials modeling at the atomic, meso, and continuum scales, Computer Physics Communications 271 (2022). https://doi.org/10.1016/j.cpc.2021.108171.

[3] L. Martinez, Andrade,R., Birgin,E.G.&Martinez,J, PACKMOL:a package for building initial configurations for molecular dynamics simulations, J. Comput. Chem 30 (2009) 2157-2164.

[4] M.R.-H. A. Menke, T. Klengel, E.B. Binder, D. Mehta, Peripheral blood gene expression: it all boils down to the RNA collection tubes, BMC Res. Notes 5 (2012) 1.

[5] W. Humphrey, Dalke, A. & Schulten, K., VMD: visual molecular dynamics, J. Mol. Graph 14 (1996) 27-38.

[6] T. Lu, F. Chen, Multiwfn: A multifunctional wavefunction analyzer, Journal of Computational Chemistry 33(5) (2012) 580-592. https://doi.org/10.1002/jcc.22885.

[7] J. Zhang, T. Lu, Efficient evaluation of electrostatic potential with computerized optimized code, Physical Chemistry Chemical Physics 23(36) (2021) 20323-20328. https://doi.org/10.1039/d1cp02805g.

[8] F.J.D. P.J. Stephens, C.F. Chabalowski, M.J. Frisch, Ab initio calculation of vibrational absorption and circular dichroism spectra using density functional force fields, J. Phys.Chem 98(45) (1994) 11623-11627.

[9] F. Weigend, R. Ahlrichs, Balanced basis sets of split valence, triple zeta valence and quadruple zeta valence quality for H to Rn: Design and assessment of accuracy, Physical Chemistry Chemical Physics 7(18) (2005). https://doi.org/10.1039/b508541a.

[10] C.J.C. A.V. Marenich, D.G. Truhlar, Universal solvation model based on solute electron density and on a continuum model of the solvent defined by the bulk dielectric constant and atomic surface tensions., J. Phys. Chem. B 113(18) (2009) 6378-6396.

[11] G. Kresse, J. Hafner, Ab initiomolecular-dynamics simulation of the liquid-metal–amorphous-semiconductor transition in germanium, Physical Review B 49(20) (1994) 14251-14269. https://doi.org/10.1103/PhysRevB.49.14251.

[12] G. Kresse, Joubert, D, From Ultrasoft Pseudopotentials to the Projector Augmented–Wave Method., Phys. Rev. B 59 (1999) 1758-1775.

[13] G. Kresse, Furthmüller, J, Efficient Iterative Schemes for Ab Initio Total-Energy Calculations Using a Plane-Wave Basis Set, Phys. Rev. B 54 (1996) 11169-11186.

[14] J.P. Perdew, Burke, K., Ernzerhof, M, Generalized Gradient Approximation Made Simple, Phys. Rev. Lett 77 (1996) 3865-3868.

[15] S. Grimme, S. Ehrlich, L. Goerigk, Effect of the damping function in dispersion corrected density functional theory, Journal of Computational Chemistry 32(7) (2011) 1456-1465. https://doi.org/10.1002/jcc.21759.

[16] H.J. Monkhorst, J.D. Pack, Special points for Brillouin-zone integrations, Physical Review B 13(12) (1976) 5188-5192. https://doi.org/10.1103/PhysRevB.13.5188.

[17] W. Fan, P. Li, J. Shi, J. Chen, W. Tian, H. Wang, J. Wu, G. Yu, Atomic Zincophilic Sites Regulating Microspace Electric Fields for Dendrite-Free Zinc Anode, Advanced Materials 36(1) (2023).

https://doi.org/10.1002/adma.202307219.
[18] L. Cao, D. Li, E. Hu, J. Xu, T. Deng, L. Ma, Y. Wang, X.Q. Yang, C. Wang, Solvation Structure Design for Aqueous Zn Metal Batteries, J Am Chem Soc 142(51) (2020) 21404-21409. https://doi.org/10.1021/jacs.0c09794.
[19] Z. Shi, M. Yang, Y. Ren, Y. Wang, J. Guo, J. Yin, F. Lai, W. Zhang, S. Chen, H.N. Alshareef, T. Liu, Highly Reversible Zn Anodes Achieved by Enhancing Ion-Transport Kinetics and Modulating Zn (002) Deposition, ACS Nano 17(21) (2023) 21893-21904. https://doi.org/10.1021/acsnano.3c08197.
[20] X. Bai, Y. Nan, K. Yang, B. Deng, J. Shao, W. Hu, X. Pu, Zn Ionophores to Suppress Hydrogen Evolution and Promote Uniform Zn Deposition in Aqueous Zn Batteries, Advanced Functional Materials 33(42) (2023) 2307595. https://doi.org/10.1002/adfm.202307595.
[21] Z. Li, Z. Shu, Z. Shen, Y. Liu, Y. Ji, L. Luo, R. Li, Y. Cai, H. Ian, J. Xie, G. Hong, Dissolution Mechanism for Dendrite-Free Aqueous Zinc-Ions Batteries, Advanced Energy Materials (2024) 2400572. https://doi.org/10.1002/aenm.202400572.
[22] J. Zhang, Y. Liu, Y. Wang, Z. Zhu, Z. Yang, Zwitterionic Organic Multifunctional Additive Stabilizes Electrodes for Reversible Aqueous Zn-Ion Batteries, Advanced Functional Materials (2024) 2401889. https://doi.org/10.1002/adfm.202401889.
[23] K. Qiu, G. Ma, Y. Wang, M. Liu, M. Zhang, X. Li, X. Qu, W. Yuan, X. Nie, N. Zhang, Highly Compact Zinc Metal Anode and Wide-Temperature Aqueous Electrolyte Enabled by Acetamide Additives for Deep Cycling Zn Batteries, Advanced Functional Materials (2024) 2313358. https://doi.org/10.1002/adfm.202313358.
[24] S. Yang, A. Chen, Z. Tang, Z. Wu, P. Li, Y. Wang, X. Wang, X. Jin, S. Bai, C. Zhi, Regulating the electrochemical reduction kinetics by the steric hindrance effect for a robust Zn metal anode, Energy & Environmental Science 17(3) (2024) 1095-1106. https://doi.org/10.1039/d3ee02164e.
[25] Y. Xia, R. Tong, J. Zhang, M. Xu, G. Shao, H. Wang, Y. Dong, C.-A. Wang, Polarizable Additive with Intermediate Chelation Strength for Stable Aqueous Zinc-Ion Batteries, Nano-Micro Letters 16(1) (2024) 82. https://doi.org/10.1007/s40820-023-01305-0.
[26] Z. Liu, R. Wang, Y. Gao, S. Zhang, J. Wan, J. Mao, L. Zhang, H. Li, J. Hao, G. Li, L. Zhang, C. Zhang, Low-Cost Multi-Function Electrolyte Additive Enabling Highly Stable Interfacial Chemical Environment for Highly Reversible Aqueous Zinc Ion Batteries, Advanced Functional Materials 33(49) (2023) 2308463. https://doi.org/10.1002/adfm.202308463.
[27] X. Zhao, Y. Wang, C. Huang, Y. Gao, M. Huang, Y. Ding, X. Wang, Z. Si, D. Zhou, F. Kang, Tetraphenylporphyrin-based Chelating Ligand Additive as a Molecular Sieving Interfacial Barrier toward Durable Aqueous Zinc Metal Batteries, Angewandte Chemie International Edition 62(46) (2023) e202312193. https://doi.org/10.1002/anie.202312193.
[28] S. Wang, Y. Ying, S. Chen, H. Wang, K.K.K. Cheung, C. Peng, H. Huang, L. Ma, J.A. Zapien, Highly reversible zinc metal anode enabled by zinc fluoroborate salt-based hydrous organic electrolyte, Energy Storage Materials 63 (2023) 102971. https://doi.org/10.1016/j.ensm.2023.102971.
[29] X. Wang, K. Feng, B. Sang, G. Li, Z. Zhang, G. Zhou, B. Xi, X. An, S. Xiong, Highly Reversible Zinc Metal Anodes Enabled by Solvation Structure and Interface Chemistry Modulation, Advanced Energy Materials 13(36) (2023) 2301670. https://doi.org/10.1002/aenm.202301670.
[30] X. Wu, Y. Xia, S. Chen, Z. Luo, X. Zhang, Y. Lu, H. Pan, B.B. Xu, M. Yan, Y. Jiang, Transient Zwitterions Dynamics Empowered Adaptive Interface for Ultra-Stable Zn Plating/Stripping, Small 20(8) (2023) 2306739. https://doi.org/10.1002/smll.202306739.
[31] K. Xiao, L. Yang, M. Peng, X. Jiang, T. Hu, K. Yuan, Y. Chen, Unlocking the Effect of Chain

Length and Terminal Group on Ethylene Glycol Ether Family Toward Advanced Aqueous Electrolytes, Small 20(12) (2023) 2306808. https://doi.org/10.1002/smll.202306808.